Surface recovery algorithm in white light interferometry based on combined white light phase shifting and fast Fourier transform algorithms

Article *in* Applied Optics · October 2017

DOI: 10.1364/AO.56.008174

CITATIONS
46

READS
2,952

4 authors:

Quangsang Vo
Le Quy Don Technical University
18 PUBLICATIONS **106** CITATIONS
SEE PROFILE

Fengzhou Fang
University College Dublin
479 PUBLICATIONS **10,323** CITATIONS
SEE PROFILE

Xiaodong Zhang
Tianjin University
162 PUBLICATIONS **3,224** CITATIONS
SEE PROFILE

Huimin Gao
Tianjin University
8 PUBLICATIONS **207** CITATIONS
SEE PROFILE

applied optics

Surface recovery algorithm in white light interferometry based on combined white light phase shifting and fast Fourier transform algorithms

QUANGSANG VO, FENGZHOU FANG, XIAODONG ZHANG,* AND HUIMIN GAO

State Key Laboratory of Precision Measuring Technology & Instruments, Centre of MicroNano Manufacturing Technology, Tianjin University, Tianjin 300072, China
**Corresponding author: zhangxd@tju.edu.cn*

Received 2 August 2017; revised 10 September 2017; accepted 11 September 2017; posted 12 September 2017 (Doc. ID 303931); published 6 October 2017

Quality control of micro–nano structured and freeform surfaces is becoming increasingly important, which leads to challenging requirements in the measurement and characterization of rough and highly reflective surfaces. As an important measurement technique, white light scanning interferometry (WLSI) is a fast noncontact method to measure three-dimensional (3D) surface profiles. Nevertheless, the existing WLSI 3D surface reconstruction algorithms are prone to environmental vibrations and phase changes caused by reflections on the tested surface. A novel peak detecting algorithm that combines the white light phase-shifting interferometry (WLPSI) method and fast Fourier transform (FFT) coherence-peak-sensing technique is proposed in this paper, which can accurately determine the local fringe peak and improve the vertical resolution of the measurement. A microcomponent (10 μm standard step height) and a spherical surface were used as test specimens to evaluate the proposed method. Both simulated and experimental results show that the proposed algorithm improves the precision and anti-interference ability of the WLPSI and FFT methods, which can effectively reduce the batwing effects at the edges and solve the problem of positioning error in the maximum modulation.

OCIS codes: (120.3180) Interferometry; (120.6650) Surface measurements, figure; (120.3930) Metrological instrumentation.

https://doi.org/10.1364/AO.56.008174

1. INTRODUCTION

Precision small-scale optical components are widely used as critical parts in emerging technologies [1]. The rapid development and extensive applications of optical and microelectromechanical systems (MEMS) demand advanced detection techniques with extreme accuracy. White light scanning interferometry (WLSI) is an established method for highly resolved 3D measurements of microscopic structures owing to its theoretically unlimited unambiguous range [2]. Based on spectrally broadband, short optical coherence length light, WLSI is a noncontact measurement method that can be used to characterize the surface topography of MEMS [3]. Owing to its excellent ability to resolve phase ambiguity and limit the height difference of two adjacent points closer than $\lambda/4$, the surface recovery algorithm of vertical scanning white light interferometry (WLI) is a pivotal and widely researched technique. This algorithm provides effective means for measuring structures, as the zero fringe order can be unambiguously determined, enabling the generation of an accurate surface profile [4].

Considering accurate 3D profile measurements, numerous works on the use of WLSI for surface profiling can be found in the literature. So far, demodulation techniques for WLSI signals can be basically classified into three groups, depending upon which distinctive point they pursue as the peak of interferograms: (1) The first one identifies the fringe peak that corresponds to the maximum crest of the interference intensity varying in a sinusoidal pattern; (2) the second one seeks the summit of the envelope profile of the sampled interference intensity, which is hereafter termed the envelope peak; (3) the third one is a combination that solves the envelope peak and identifies the fringe peak to improve the efficiency and accuracy of the measurement [5].

The white light phase-shifting interferometry (WLPSI) algorithm proposed by Sandoz *et al.* [6] combines traditional phase-shifting interferometry (PSI) and WLI by calculating the phase value of the peak point by using the PSI algorithm, and obtaining the result from the peak point and the phase value [7]. Owing to its high speed and simplicity, the

WLPSI algorithm had been extensively adopted in optical metrology. Unfortunately, because of its poor anti-interference ability, a problem of locating errors in the maximum modulation in the system exists. Therefore, this method cannot lead to high-precision measurements without interference. In order to obtain WLPSI with high accuracy and good anti-interference ability, a variety of WLPSI algorithms have been developed. In 2011, Gonzales *et al.* [8] introduced a simple technique to find the optimum phase shift, which maximizes the signal-to-noise ratio in the demodulated phase, for linear tunable phase-shifting algorithms (PSAs). Bhushan *et al.* [9] proposed a method to determine the height of rough and mirror-like surfaces with a three-step PSA. Shen *et al.* [10] locally linearized a five- or seven-step PSA that can be used to retrieve the WLSI signal coherence function and to determine the position of zero optical path difference (ZOPD). However, these improved PSI methods presented still seriously suffer from various sources of error. In fact, in the PSI algorithm it is difficult to control the inherent phase error, which results in a positioning error in the maximum modulation. Although in WLPSI the sources of phase errors are difficult to suppress physically, researchers have tried to overcome the phase error by improving the algorithm [11,12].

Nevertheless, white light vertical scanning interferometry (WLVSI) is able to overcome the problem of phase ambiguity by providing effective means for measuring such structures, as the zero fringe order can be unambiguously determined, enabling the generation of an accurate surface profile. Based on the transfer and analysis of signal intensity in the frequency domain, a fast Fourier transform (FFT) method was proposed by Chim and Kino [13] to filter out the high-frequency part, to obtain a coherence envelope. Subsequently, the FFT method was confirmed that can accurately locate ZOPD by solving the white light signal envelope. However, a common drawback of this technique is the enormous amount of computation required for calculating the contrast for each point in real time. The diffraction effect at the discontinuity causes the coherence envelope of the correlogram to skew and the peak to shift. Many different techniques have been used for these profilers to speed up the FFT analysis. Interferograms obtained by Muhamedsalih *et al.* [14] from a Linnik interferometer have been analyzed by FFT method. Based on windowed Fourier transform (WFT), Ma *et al.* [15,16] proposed an algorithm to retrieve the phase from the WLI that compensates for the difference from the ZOPD position. In 2013, Wang *et al.* [17] presented a nonlinear wavelength sampling algorithm in the FFT WLI that can effectively reduce the deviation in phase shift.

However, comparing all the WLPSI and FFT methods mentioned above, due to unstable systems and the sources of phase errors, such as the scanning step error and low-frequency vibration, the maximum modulation position is often determined incorrectly and the accuracy of recovery is obviously reduced, directly influencing the results of interferometry. Therefore, the most important problem to be solved in the WLI algorithm is the improvement of the accuracy of determining ZOPD, which can result in good anti-interference ability and high accuracy without the batwing effect. Based on this, several authors have done studies that combine different WLI methods and overcome the limitations of these WLPSI and WLVSI techniques. In 1996, Larkin [18] combined methods with a new procedure for ZOPD prediction using a weighted least-squares fit (LSF) method that removes the residual second-harmonic error in the envelope. In addition, the fully compensating five-step PSA was used to have much smaller errors than traditional WLPSI algorithms. In 2000, Harasaki *et al.* [19] combined PSA and coherence-peak sensing technique to calculate ZOPD positions from the best focus frame by use of least-squares fitting of the modulation contrast. In 2006, De Groot *et al.* [20] combined phase and coherence information for improved precision in the WLI algorithm. Their approach is to analyze the difference or phase gap between the phase data and coherence data techniques, using data filtering, connecting of the phase gap, and surface fitting. In order to address the problems above, a new algorithm for WLSI measurement is presented in this paper to avoid incorrect detection of coherence peak positions, which combines WLPSI and FFT coherence peak sensing techniques by attempting to solve the problem of positioning error in the maximum modulation effectively and removing the batwing effect at the step edges.

In this algorithm, high-speed WLPSI measurements are used to determine the maximum modulation of the WLI interference signal and to identify the coarse profile of the test surface regions separated by a large step. By the determination of surface discontinuities, we calculated to correct for slight displacements and phase shifts that may have occurred. Within the range of surface discontinuities, by correlation analysis of the WLI envelope curves, the FFT method can be used to reposition the maximum modulation. Finally, by using a polynomial three-point fitting method, the estimated Fourier peak positions were accurately determined, the series of height values based on these reference positions were obtained, and the final surface height was determined from the average of these height values. To a certain extent, this method effectively overcomes the disadvantages of the traditional WLPSI and FFT methods, which can improve the accuracy of height measurements in steep regions and in areas with large interpixel steps on the test surface.

To evaluate the performance of the algorithm, a simulation was performed with ideal height values with random noise. Specimens such as a step height standard and a spherical surface were measured by difference scanning step interval by using a Mirau interference microscope developed by us to test the performance of the proposed method. By a series of computational simulations and experiments, the proposed method showed its effectiveness in improving noise immunity, calculation efficiency, and accuracy.

This paper is arranged as follows: Section 2 outlines the essential details of the configuration and the principles of WLSI and describes the detection of phase and fringe peaks by WLPSI. Furthermore, by using the FFT method, the peak position of the envelope of the correlogram is determined. Concurrently, a new algorithm that combines the WLPSI and FFT coherence-peak sensing techniques is proposed. Section 3 compares the envelope detection methods using the new algorithm with traditional WLPSI and FFT algorithm. The important features of peak detection schemes are compared. Section 4 proposes an optical interference measurement system, which is used to experimentally evaluate the feasibility

and effectiveness of the new algorithm. Section 5 concludes the paper.

2. PRINCIPLES

WLSI is a noncontact, optical technique for measuring surface height and shape with high speed and accuracy. A typical Mirau interferometer setup can be used for a WLSI system with a microscope arrangement, as shown in Fig. 1. In this setup, a broadband light source provided a beam that was passing through a filter and was reflected by the upper beam splitter down to the objective lens of the Mirau interferometer. By using a piezoelectric transducer (PZT) for vertically moving the objective in the nanometer range, the path length between the sample and the beam splitter can be varied and a series of moving interference fringes can be created, which can be detected by a CCD camera. The system uses a series of advanced computer algorithms to record the exact vertical positions for each point on the surface with nanometer resolution.

The system setup and the obtained sample interferogram are shown in Fig. 1(a).

As described above, the PZT translator is used for moving the Mirau interferometer in the vertical direction with a specific interval. The interferogram was taken at each height position and the intensity of the interferogram was captured as well. The dependence of intensity on the depth is illustrated in Fig. 1(b).

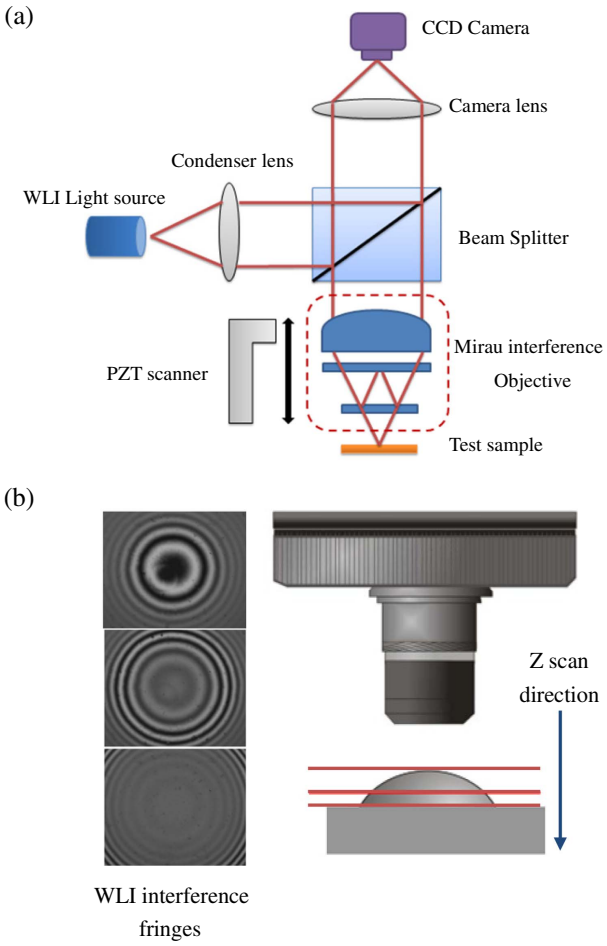

Fig. 1. (a) Schematic of the WLI system and (b) illustration of WLI interference fringes.

In WLI, the intensity function of a point on the specimen recorded by the camera along the vertical scanning direction can be written as [21,22]

$$I(z) = I_B + \gamma I_B \exp\left[-\left(\frac{z - z_0}{l_c}\right)^2\right] \cos\left[\frac{4\pi}{\lambda_0}(z - z_0) + \varphi_0\right], \tag{1}$$

where I_B is the background intensity; γ is the fringe contrast; l_c is the coherence length of Gaussian spectrum light source; z is the scanning position along optical axis; λ_0 is the center wavelength; z_0 is the position along the scanning direction where the envelope of WLI signal is maximum; and φ_0 is the phase difference between the reference and object light beams introduced by the optical system. For convenience, Eq. (1) can also be rewritten as

$$I(z) = I_B\{1 + \gamma g(z)\cos[\phi(z)]\}, \tag{2}$$

where $g(z) = \exp[-(z - z_0)^2/l_c^2]$ is the envelope function of the WLI signal; and $\phi(z) = 4\pi(z - z_0)/\lambda_0 + \varphi_0$.

Therefore, the recorded peak position of the WLSI signal may not be the actual ZOPD position. The relationship of recorded intensity peak z_0 and actual ZOPD position z_0 can be calculated as

$$z_0 = z' - \frac{\lambda_0}{4\pi}\phi(z'), \tag{3}$$

where $\phi(z')$ is the phase of z' used for the compensation of the ZOPD [21].

Based on the WLPSI method, data processing for the white light interferometric measurement involves scanning the locations of ZOPD, which provide the surface height. Thus, to retrieve the height information of a test sample, the ZOPD fringe position should be identified accurately. By moving the PZT, an additional phase difference was introduced between the reference and the object beams, and the WLPSI method was used to extract the phase value and peak position of the recorded WLSI signal. Therefore, to measure the fractional phase from the best focus frame position, the frame position with the maximum modulation contrast of the correlogram has to be found first; then, a mathematical algorithm can be applied to recover the phase information.

However, because of the reflection phase change and the existence of disturbance sources such as the scanning step error and low-frequency vibration, the envelope peak does not coincide with the fringe peak, which represents the actual peak of the fringe intensity following a sinusoidal pattern [23]. Obviously, the WLPSI method depends on the phase change of the interference light intensity, and the accuracy of the measurement is higher than that of the light intensity, which is sensitive to noise, and as a result the position of the maximum modulation is often incorrectly determined. From Fig. 2, it is clear that the discrete sample zero-order fringe peak position h^* identified by the WLPSI method is not necessarily the same as the "true" ZOPD position h, which requires the use of other auxiliary methods that can accurately determine the position of the ZOPD.

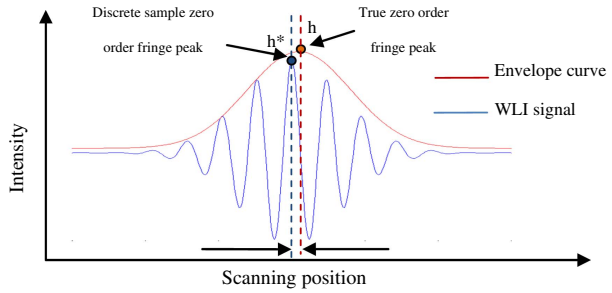

Fig. 2. Illustration of the "true" zero-order fringe peak and discrete sample zero-order fringe peak of the WLI signal.

Based on this knowledge, compared with the current algorithms in WLSI, in this research a new signal processing WLI algorithm is proposed for determining the surface discontinuities and correcting the errors in the obtained fringe order. This new method, using a combination of WLPSI and modified FFT coherence-peak sensing techniques has been proposed and investigated theoretically, and it can provide correct surface height measurements when the object under investigation has a step-like discontinuity with a height less than the coherence length of the broadband light source.

The process of the proposed algorithm is as follows:

Step 1: Obtain the maximum modulation of interference signal at each pixel by using WLPSI. The position and phase of the maximum modulation in the system are determined; thus, the zero optical path position of the interference signal is obtained.
Step 2: From the WLI principle, the light reflected from the surface forms interference fringes, with the period of one fringe $\lambda/2$ of the surface height. The relationship between two adjacent data points of the ZOPD can be determined from the height difference between the adjacent points by the following condition:

$$|H(j+1) - H(j)| \geq \frac{\lambda}{2}. \tag{4}$$

It is assumed that there is an error in the zero optical path position of WLPSI, or the surface is discontinuous at this point. The white light scanning interferometric signal has to be determined by FFT, and the maximum modulation position has to be relocated.
Step 3: The envelope and the phase of the white light scanning interference signal are obtained by the FFT method. The envelope of the intensity response is extracted, and the maximum modulation position of the envelope corresponding to the zero-order fringe is identified.
Step 4: By identifying the Fourier peak in Step 3, a parabolic direct quadratic polynomial fitting on three data points around the Fourier peak is used. As the slope at the peak of the curve is equal to zero, the Fourier peak position can be calculated, which is used to calculate the surface height.

The new algorithm is developed, as shown in Fig. 3.

A. Detection of Fringe Peaks by WLPSI Algorithm

First, by using the WLPSI algorithm, the peak of the visibility function has to be found, which can be identified from the white light interferogram. As the coherence length of the

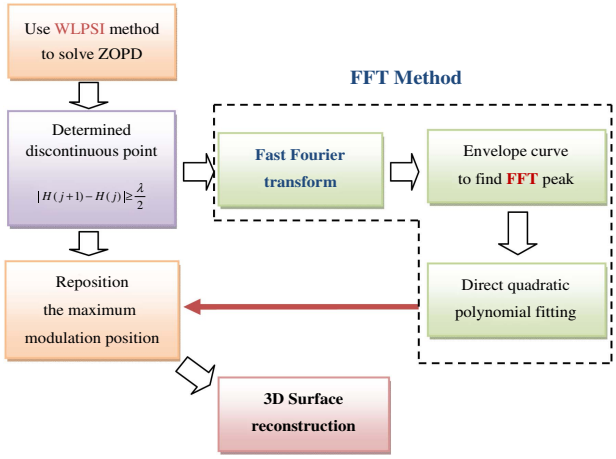

Fig. 3. Flow chart of the proposed WLI algorithm.

two white lights is narrow, the WLPSI of the phase information with respect to the visibility changes along the scanning direction. To obtain the position of the maximum fringe contrast to locate the maximum intensity, the visibility V and the phase ϕ are calculated at each step of the scanning, by using the following expression [24,25]:

$$V_j^2 = (I_{j-1} - I_{j+1})^2 - (I_{j-2} - I_j)(I_j - I_{j+2}). \tag{5}$$

Then, the phase difference ϕ between the ZOPD and the best-focus scanning position is determined by using a five-bucket WLPSI algorithm, which can be calculated as

$$\phi_j = \tan^{-1}\frac{\sqrt{4(I_{j-1} - I_{j+1})^2 - (I_{j-2} - I_{j+2})^2}}{-I_{j-2} + 2I_j - I_{j+2}}, \tag{6}$$

where I_j are the five consecutive intensity data at each pixel, as shown in Fig. 4. The phase ϕ_j obtained from Eq. (6) is a wrapped phase, which is often discontinuous and needs to be unwrapped as a continuous phase distribution ϕ_j'. Finally, the topography of the surface of height is obtained by

$$H = \frac{\lambda}{4\pi} \times \varphi_j', \tag{7}$$

where λ is the WLI light source of the center wavelength.

As described in the method above, when modulation V is maximal, the best-focus scanning frame position (step number) can be determined. Therefore, WLPSI combines the intensity

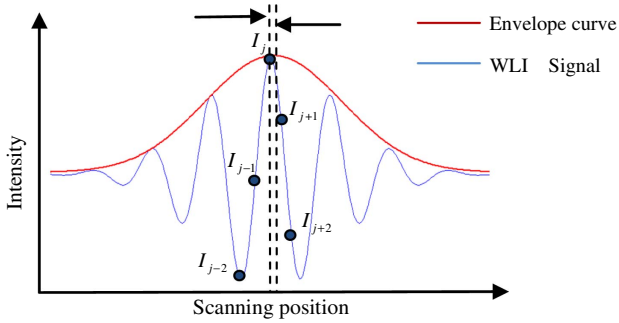

Fig. 4. WLPSI algorithm.

information and phase information of interference signals to locate the coherent peaks, thus improving the measurement efficiency. Unfortunately, because of the reflection phase change and the existence of disturbance sources such as a scanning step error, low-frequency vibration, and material properties of the object such as tilt, numerical aperture of the lens, etc., the position of maximum modulation is not always on the fringe of the ZOPD. From the fundamental WLI principle, the light reflected from the surface forms interference fringes, and the period of one fringe is $\lambda/2$ of the surface height. In order to determine whether the maximum modulation position is the correct ZOPD position, the location of the ZOPD is compared between adjacent data points. This relationship is determined as

$$|H(j+1) - H(j)| \geq \frac{\lambda}{2}, \tag{8}$$

where $H(j+1)$ and $H(j)$ define the height of two adjacent data points and λ is the center wavelength of the white light source. When the above relationship in Eq. (8) is satisfied, the position of maximum modulation was incorrectly located, therefore causing a discontinuity on the surface. In such a case, the ZOPD position has to be relocated by using the FFT method and the ZOPD calculated by the WLPSI formula. Obviously, the FFT envelope method is only applied when the location of the position of maximum modulation is incorrectly determined by the WLPSI and leads to a discontinuity on the surface area. In this way, a lower amount of computation improves the anti-interference ability of the algorithm.

B. Reposition of the Position of Maximum Modulation by FFT Method

If the conditions in Eq. (8) are satisfied, the surface can be considered as discontinuous. In this case, the white light scanning interferometric signal has to be obtained by using the FFT method, and the position of maximum modulation has to be relocated. To determine the position of the highest contrast, which corresponds to the surface height, the phase information of the FFT correlogram is used.

According to Eq. (1), the FFT of the WLI signal is expressed by [26,27]

$$\mathrm{FT}[I(z)] = 2\pi I_B \delta(k) + G(k)e^{-hkj}\gamma * \frac{1}{2}\left[e^{\varphi j - \frac{4\pi h}{\lambda_0} j}\delta\left(k - \frac{4\pi}{\lambda_0}\right) + e^{-\left(\varphi j - \frac{4\pi h}{\lambda_0} j\right)}\delta\left(k + \frac{4\pi}{\lambda_0}\right)\right], \tag{9}$$

where $\delta(k)$ is the impact function; $G(k)$ is the Fourier transform of $g(z-h)$; the asterisk describes convolution; $k = 2\pi/z$ is the spatial angular frequency; and $4\pi/\lambda$ is the carrier angular frequency in radians. Thus, a spectral analysis can be performed by using Eq. (9), which contains equal amounts of positive and negative frequencies and the zero-frequency components in the middle. Remove the negative frequencies and the zero-frequency components and move the positive frequency to the center of the amplitude frequency curve. By using inverse FFT, the following relation can be obtained [28]:

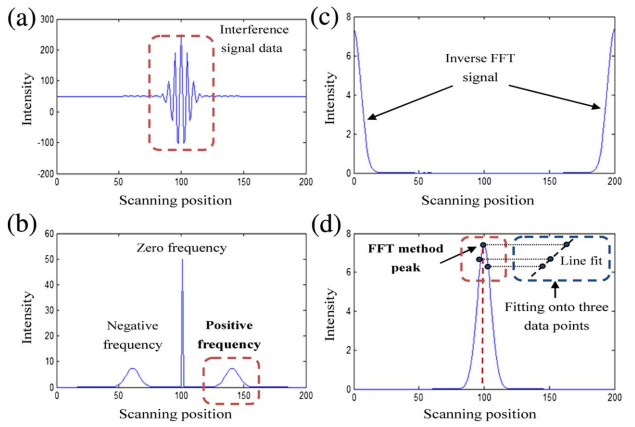

Fig. 5. Repositioning the maximum modulation position by FFT method. (a) Original WLI signal. (b) FFT spectrum that contains equal amounts of positive and negative frequencies and the zero-frequency components in the middle. (c) Inverse FFT for the positive frequency components. (d) The FFT peak location can be found by using a fit to a Gaussian curve.

$$\mathrm{IFT}\left[\frac{\gamma}{2}e^{\varphi j}G(k)e^{-khj}\right] = \frac{\gamma}{2}e^{\varphi j}g(z) * \delta(z-h) = \frac{\gamma}{2}e^{\varphi j}g(z-h). \tag{10}$$

Obviously, the envelope curve $g(z-h)$ of the WLI signal is directly proportional to the amplitude in Eq. (10). Therefore, a Gaussian fit is used to determine the precise peak position of the envelope from where the surface height H can be obtained.

The FFT method can be explained through a simulated case, as shown in Fig. 5. As shown in Fig. 2(a), according to Eq. (1), a WLSI signal was first generated with parameters $\lambda_0 = 550$ nm, $z_0 = 100$ nm, $I_B = 200$, $\gamma = 1$, $\varphi_0 = 0$, and l_c was set to be 60 nm. The PZT scanning increment was set as $\Delta z = 50$ nm.

In order to determine the FFT peak accurately, the fitted spectrum was used to determine the phase shift. Then, by using a parabolic fitting via three data points around the FFT peak, phase variations of less than 2π were detected.

3. SIMULATION RESULTS

In WLSI, the series of interferograms were obtained while the test object is scanned vertically along the z axis. For a simulational comparison between the proposed algorithm and the traditional WLPSI and FFT algorithms, a set of simulated WLI interferometric coherent data is tested. The generated discrete white light signal $I(n)$ is described as follows:

$$I_n = 200 + 200\exp\left[-\frac{(n-50)^2\Delta^2}{\sigma^2}\right]\cos\left[\frac{4\pi}{\lambda_0}(n-50)\Delta + \phi_0\right], \tag{11}$$

where Δ is the scanning step 50 nm; σ is set to be 500 nm ($\sigma = l_c/2\pi$, l_c is the coherence length of the light source); and ϕ_0 is an additional phase term due to different reflections. The center wavelength of the WLI source was set to $\lambda_0 = 550$ nm. The coherence peak of the simulated continuous

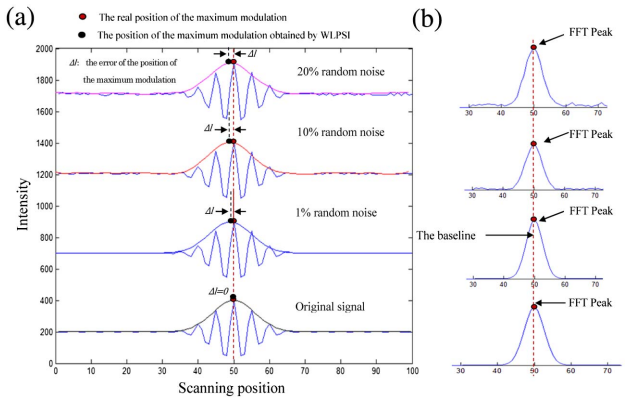

Fig. 6. Determining the simulated position of maximum modulation by WLPSI and FFT method. (a) Maximum modulation envelope curve obtained by WLPSI. (b) ZOPD position relocated by the FFT method.

signal was located at 50, and the corresponding surface height was 3000 nm.

In Fig. 6, four different series of fringe patterns can be seen with random noise restricted to 0%, 1%, 10%, and 20% of the maximum fringe intensity for a scanning increment of 50 nm. Figure 6(a) shows the application of WLPSI to determine the maximum modulation of the interference signal at each pixel. The position and phase of the maximum modulation in the system were determined; thus, the ZOPD position of the interference signal is obtained. It can be seen that as the random noise increases, the error of the position of the maximum modulation also increases. For the relocation of the ZOPD, Fig. 6(b) shows the point of discontinuity on the surface. The ZOPD position of the WLSI signal is identified by the FFT method, as described in Section 2.B. The error in ZOPD includes the phase change, due to reflection and random noise obtained by WLPSI, can accurately be determined by the estimated Fourier peak position.

As depicted in Fig. 6(a), a WLSI signal was first generated with random noise, with the scanning interval set to $\Delta = 50$ nm. To retrieve the height value of the simulated test sample, the ZOPD position has to be identified. The simulated WLI signal adds a 20% random noise, and the surface height was calculated 20 times at the same conditional by WLPSI, FFT, and the proposed method. The results of the calculations are shown in Table 1.

A comparison of calculation results and processing speed for traditional WLPSI, FFT, and the proposed method is shown in Table 1. It can be seen that due to the frequency of the transformation, the calculation of the FFT method is the slowest.

Table 1. Comparison of Calculation Results and Processing Speed of Each Algorithm

Algorithm	Height (μm)	Time (μs)	Absolute Error	Relative Error
Traditional WLPSI	3.065	35.5	0.065	2.16%
FFT method	3.033	2205	0.033	1.10%
Proposed method	3.015	56.5	0.015	0.50%

Moreover, the change of light intensity and direct current has a great influence on the calculation accuracy in the actual sampling process. Although WLPSI is a simple and high-speed calculation, because of the poor anti-interference ability, the problem of locating errors in the maximum modulation causes the reduction of the accuracy of this method. The improved algorithm subtracts the average light intensity before the calculation in order to reduce the influence of the direct current signal in the interference light intensity on the calculation accuracy, so the calculation precision is higher and the computation time is shorter. Considering the accuracy of the algorithm and computational time, the proposed algorithm is more efficient and practical.

For further analysis, a simulated WLI signal with 10% Gaussian noise is generated and calculated again by using the three algorithms above. The results of surface height are shown in Fig. 7.

To investigate the relationship between the results from the measurement and the system noise, the WLI signal noise was superimposed with ideal simulation data. As can be seen from Fig. 7, for the simulated cases containing noise, the computed results of ZOPD (the height) determined from both the FFT and the proposed method were better than those of the traditional WLPSI method. The reason was that WLPSI did not predict the accurate initial peak location, and this subsequently resulted in a large error. The proposed method was more accurate than the other two algorithms, and it was better than FFT in measurement speed. In order to study the influence of noise on the proposed algorithm, different noise levels for the WLI signal were simulated. Using a scanning increment of 20 nm, WLI fringe patterns with random noise reduced to 0%, 5%, 10%, 15%, 20%, 25%, 30%, and 35% of the maximum fringe intensity were generated. The surface height was calculated by WLPSI, FFT, and the proposed method; the simulation results are shown in Fig. 8.

Figure 8 shows a comparison of RMS errors, which were introduced by the three different methods. The RMS errors decreased significantly as the random noise of the WLI signal was increased. It can be seen that the proposed WLI algorithm was almost immune to the noise, while the errors introduced by the traditional WLPSI and FFT method increased significantly as the noise increased. Therefore, it can be seen that the

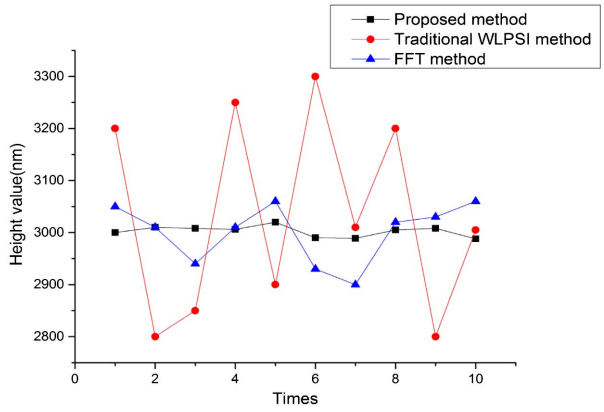

Fig. 7. Results of surface height values of simulated WLI signal with 10% Gaussian noise.

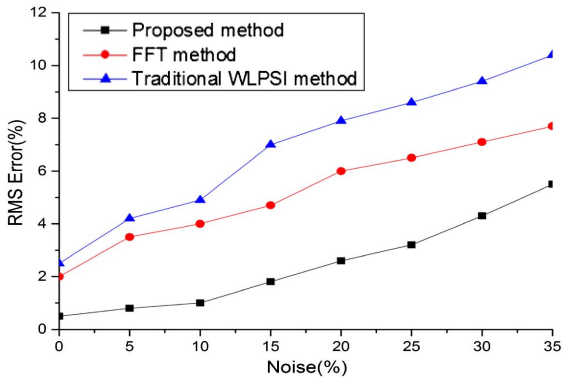

Fig. 8. Comparison of RMS errors due to different random noise levels.

proposed algorithm was the most stable, while environmental factors had the greatest effect on the traditional WLPSI algorithm and the second greatest effect on the FFT algorithm.

In the WLSI method, the scanning step was one of the important parameters of WLI. However, in the actual measurement, an ideal degree of precision of the scanning mechanism was difficult to achieve, and the completion time of the measurement would be increased with the decrease of the scanning step; therefore, an appropriate scanning step had to be considered to ensure the efficiency and accuracy measurement at the same time. Accordingly, the influence of the scanning increment was also investigated, based on a fringe pattern when a 20% random noise was introduced. By using WLPSI, FFT, and the proposed method, the relationship between the RMS errors with the scanning step is shown (Fig. 9).

As can be seen in Fig. 9, as the scanning interval increased, the error remained relatively constant. With the increase of the scanning step, the error changed subtly, the RMS error of the proposed algorithm and the FFT method increased rapidly; especially when the scanning step was larger than 100 nm, the error increased steeply. Among these methods, the scanning step had little influence on the proposed method, and when the scanning distance increased, the measurement accuracy was better. Therefore, considering the measurement accuracy and measurement efficiency, the scanning distance of 20–60 nm was a better choice for the proposed algorithm. Overall, the above comparison of results demonstrates the high accuracy of the method proposed in this paper.

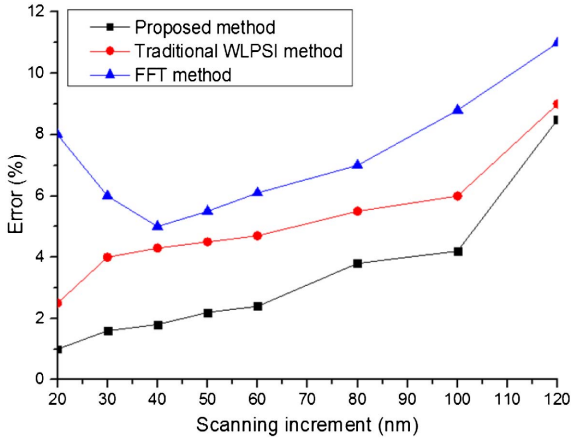

Fig. 9. Comparison of errors due to scanning increment.

4. EXPERIMENTAL VERIFICATION

To verify the simulated results by the proposed algorithm, our experimental WLI setup is shown in Fig. 10. A Mirau-type interferometric microscope with an objective lens with magnification of 20× and numerical aperture of 0.4 was used to capture the interferogram, which was recorded by a CCD camera with a resolution of 640 pixels × 480 pixels and frame rate of 30 Hz, through an imaging lens. A PZT nanoposition stage (P-841.10, Physik Instrumente, Germany) and an X–Y translation stage (Thorlabs, MSC202, U.S.) controlled by high-precision motion control (BBD202 of Brushless DC Motor Control) were used to move the specimen vertically and horizontally, respectively. The PZT was able to achieve a 0.3 nm scanning resolution and was controlled by a servo-controller (E-625.SR, Physik Instrumente, Germany). A PZT translator for moving the objective vertical scanning in nanometer range, and the CCD camera (SCA1300, Ximea, Germany) was used to capture a series of interferograms. The light source was a halogen lamp with a broad continuous spectrum. The object was mounted on a PZT stage, controlled by a computer to move it along the z direction with a specific interval. For each nanometer scale increment, the CCD recorded one fringe pattern and stored it in a computer. A series of fringe patterns were analyzed and a 3D profile of the test object was obtained.

A. Measurement of the 10 μm Standard Step Height

First, in order to show the accuracy of the testing system with our proposed method, a 10 μm standard step height (9.976 ± 0.028 μm) manufactured by VLSI Standards Inc. and calibrated by the National Institute of Standards and Technology (NIST) was measured 10 times. The light source was a white light illuminator (center wavelength of 550 nm), the scanning range was configured to be 20 μm, and the scanning step was 50 nm. The CCD camera was used to capture a

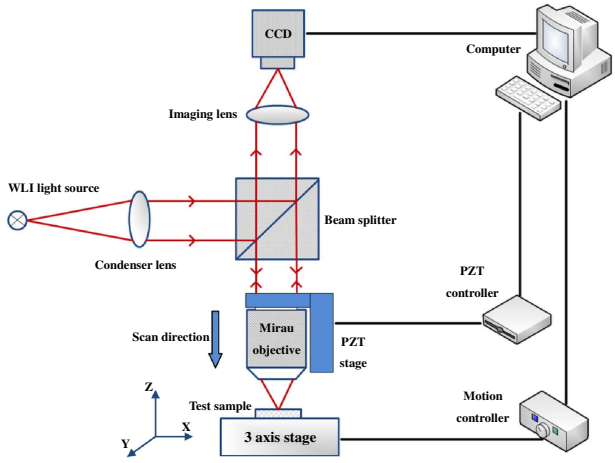

Fig. 10. Schematic of experimental arrangement for the proposed WLI algorithm.

series of patterns while the PZT stage moved the test object along the scanning direction.

The obtained 3D structure and a section profile of the result are shown in Fig. 11, and the obtained step values are shown in Table 2. The height value was obtained by fitting the measurement data of the upper and lower surfaces. It can be seen that the mean height value is 10.014 μm, while the standard deviation is 0.020 μm. The experimental results show that the proposed algorithm is in good agreement with the specifications, which indicates that the instrument was well calibrated.

In order to compare traditional WLPSI, FFT, and the proposed method, the WLI measurement system described above was used to measure a standard step height of 10 μm. For the scanning step of 50 nm, a series of WLI interferograms were captured by the CCD camera for the standard step sample. The captured frames were analyzed by the previously described four-bucket and five-bucket WLPSI, FFT, and the proposed methods. Figure 12 shows the 3D microprofile measurement of the standard step height obtained by the three methods. In Figs. 12(a) and 12(b), the step height profile shows many discontinuities, indicating measurement errors. Indeed, during the vertical scanning, because the step discontinuities are lower than the coherence length, the light diffracted by the top edge and the light reflected from the bottom will interfere with each other, and then travel back to the interferometer. This phenomenon is called the batwings effect at the edge. Figure 12(c) shows that the FFT method had obvious batwing effects, and the measurement result can be distorted by diffraction at the sharp edge of the step height. However, as shown in Fig. 12(d), a smoothened and continuous profile was obtained by using the proposed algorithm.

As shown in Figs. 13(a) and 13(b), without our method to determine the fringe order, the measurement result was distorted at the edge of the step height standard. However, it can be seen in Fig. 13(c) that the measurement result was not distorted when the proposed method was used. At a sharp edge of the step height sample, the new algorithm can correct the fringe order determined incorrectly. The explanation for this is that the traditional WLPSI and FFT methods retrieve the surface height by locating a local fringe peak and a global envelope peak, respectively.

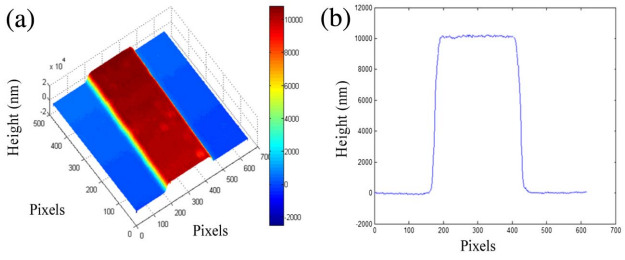

Fig. 11. Results for a 10 μm step height standard measurement: (a) 3D display and (b) 2D cross-section profile.

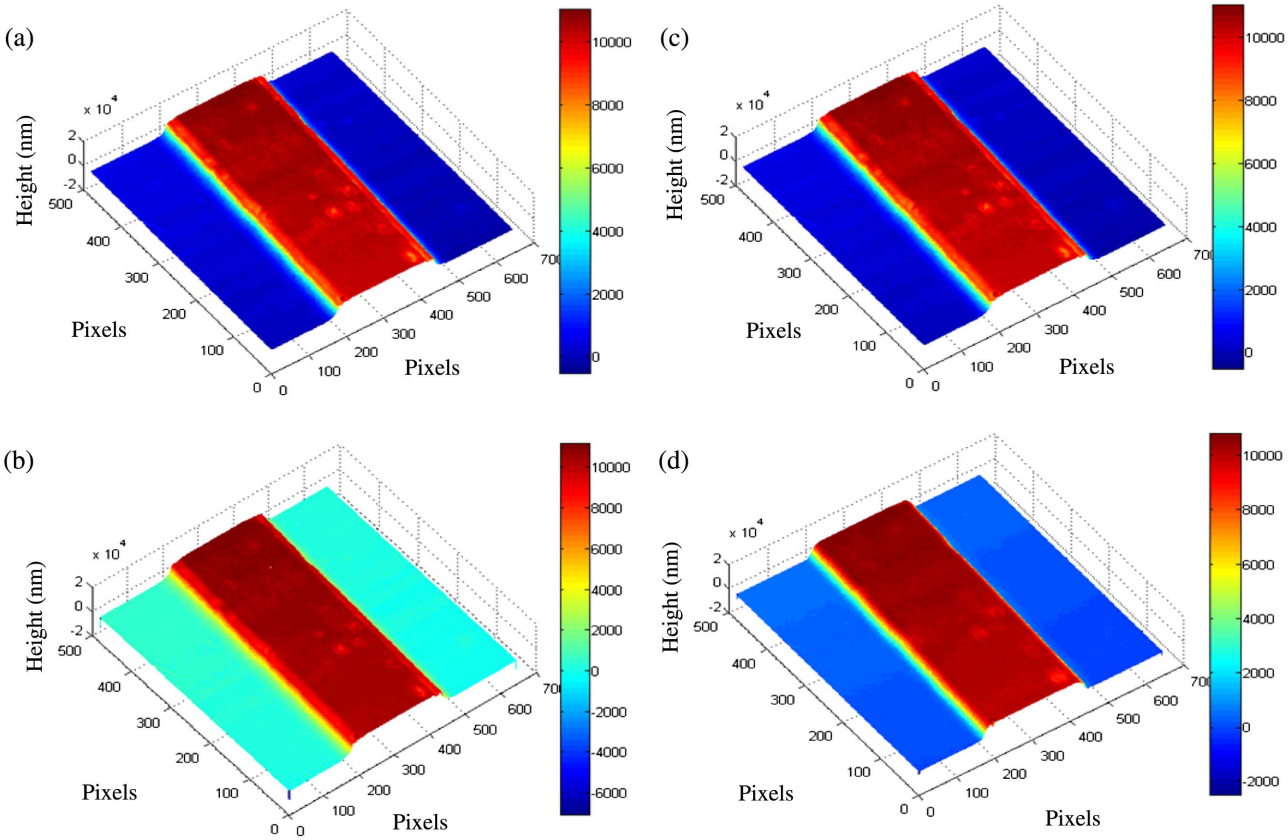

Fig. 12. 3D structure of the 10 μm step height standard using different algorithms: (a) by using four-bucket WLPSI algorithm, (b) by using five-bucket WLPSI algorithm, (c) by using FFT algorithm, and (d) by using the proposed algorithm.

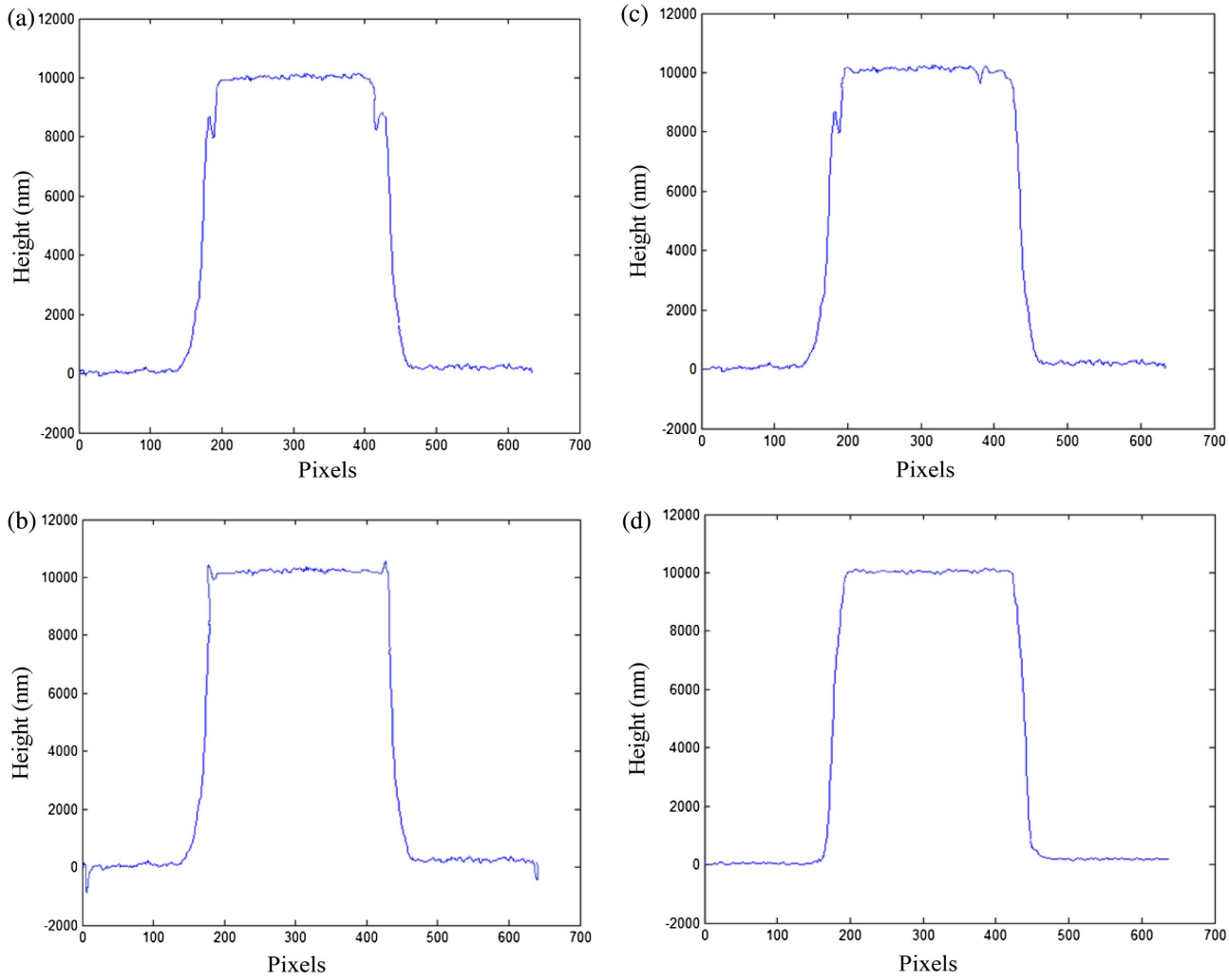

Fig. 13. Surface profile of the 10 μm step height standard using different algorithms: (a) by using four-bucket WLPSI algorithm, (b) by using five-bucket WLPSI algorithm, (c) by using FFT algorithm, and (d) by using the proposed algorithm.

The proposed method that combines the WLPSI and the FFT methods, which can exploit the advantages of both local and global approaches, is, therefore, capable of determining the ZOPD points accurately by repositioning the location of the maximum modulation. The results show that the performance of the proposed algorithm is better than that of the WLPSI and FFT methods.

In order to evaluate the performance of the proposed algorithm by a large field measurement, two continuous 10 μm standard step height surfaces were scanned and evaluated by the use of the previously described WLI measurement system.

Figure 14 shows the top view of the two continuous standard step height surfaces. By using the three methods above, the 3D surface plot of the two continuous standard steps height surfaces was obtained, as shown in Fig. 15. The profiles along the cross sections A-B-C-D in Fig. 15(a) are shown in Fig. 15(b). The step height value was determined by the difference between the mean line value of the upper and lower surfaces. From the description above, the height difference between the points A and B (see Fig. 15) and C and D is given as 9.976 ± 0.028 μm. A comparison of the results of the distance of the surfaces from the two continuous 10 μm standard step heights by using the traditional WLPSI, FFT, and the proposed method is listed in Table 3.

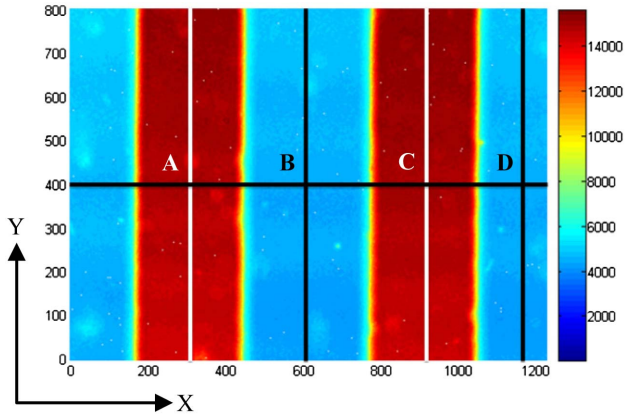

Fig. 14. 3D structure for two continuous 10 μm standard step heights.

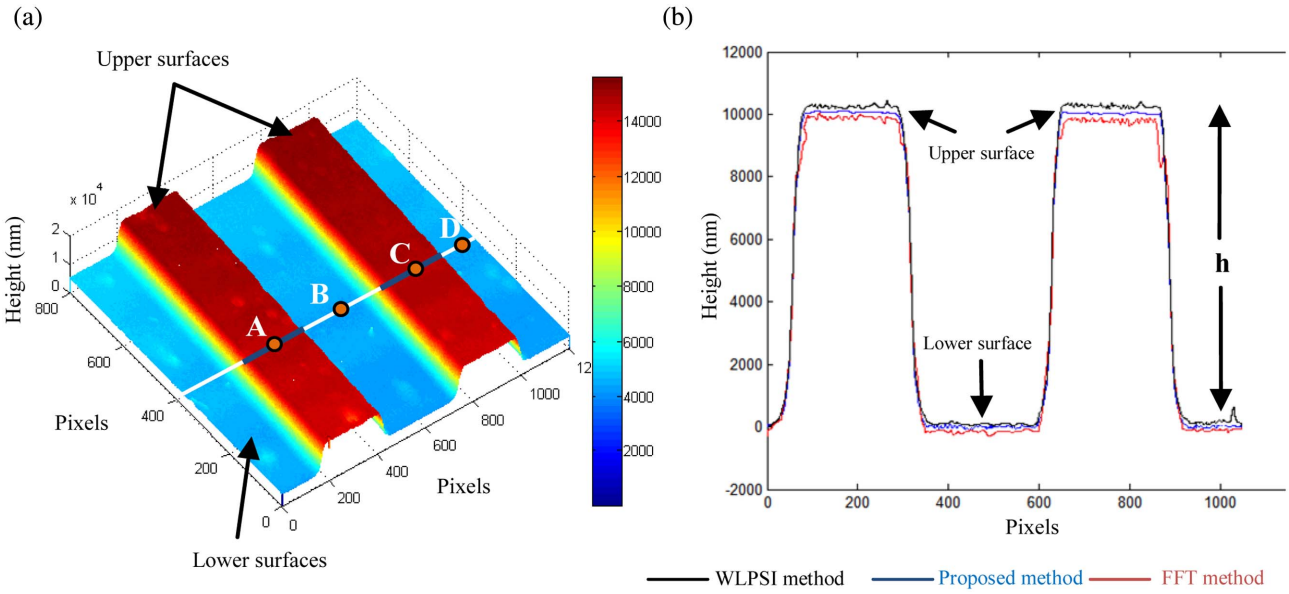

Fig. 15. (a) 3D plot of a reconstructed two continuous 10 μm standard step heights. (b) Comparison of 2D profiles obtained by the three methods.

As shown in Fig. 15(b) and in Table 3, the WLPSI, FFT, and proposed algorithms determined the average step height value as 10.395 μm, 10.088 μm, and 10.023 μm, respectively. It can be seen that the error of the step height measurement has been reduced from 0.395 μm to 0.023 μm. The maximum discrepancy between the results obtained by the proposed method and the profiler is 0.23%, while in the case of the WLPSI and FFT methods, these are 3.95% and 0.88%, respectively.

Nevertheless, it can be seen that the speed of the WLI fringe analysis using the proposed method is faster than that of the FFT and approximation WLPSI methods.

Figure 16 shows the results of the average value of the surface height h calculated 10 times by three algorithms. It can be seen that the measurement results of the proposed method are the closest to the actual height of the step.

Table 2. Results of the 10 μm Standard Step Height Calibration

Measurement Number	Height (μm)	Measurement Number	Height (μm)
1	10.027	6	10.023
2	10.029	7	10.025
3	10.021	8	10.022
4	9.971	9	10.025
5	9.977	10	10.021
Mean value (μm)	10.014		
Standard deviation (μm)	0.020		

Table 3. Comparison Measurement Results for Two Continuous 10 μm Standard Step Heights by Using the Three Algorithms

Results	WLPSI (μm)	FFT (μm)	Proposed Method
Mean of AB height	10.250	10.055	10.025
Mean of CD height	10.540	10.120	10.021
Meas. error (AB)	0.250	0.055	0.025
Meas. error (CD)	0.540	0.120	0.021
Average height value	10.395	10.088	10.023
Standard deviation	3.95%	0.88%	0.23%
Calculation time (s)	90	3260	115

B. Measurement of a Spherical Surface

Furthermore, another experimental test was carried out to verify the advantages of the proposed algorithm. As a further example of profiling, the profile of a spherical surface is presented. A spherical surface machined by a Nanotech UPL 250 ultraprecision turning machine was chosen for the verification, which had different surface gradients at different lateral

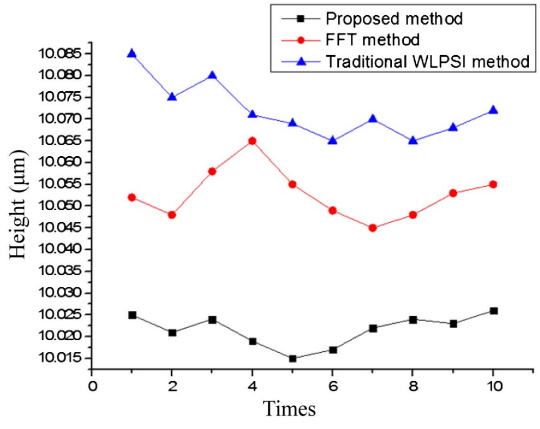

Fig. 16. Comparison of the results from the two continuous 10 μm standard step heights by the three algorithms.

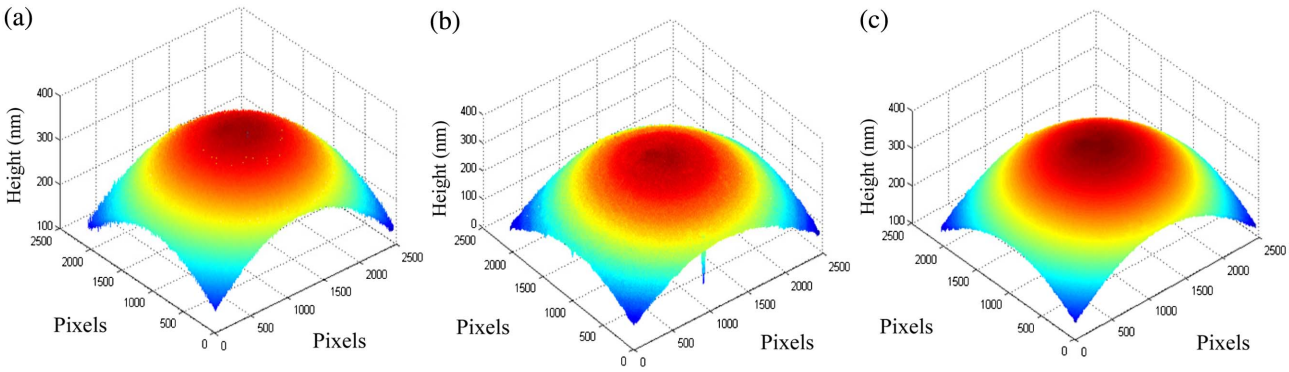

Fig. 17. 3D structure of the spherical surface simulated by three different algorithms: (a) by using traditional WLPSI algorithm, (b) by using FFT algorithm, and (c) by using the proposed algorithm.

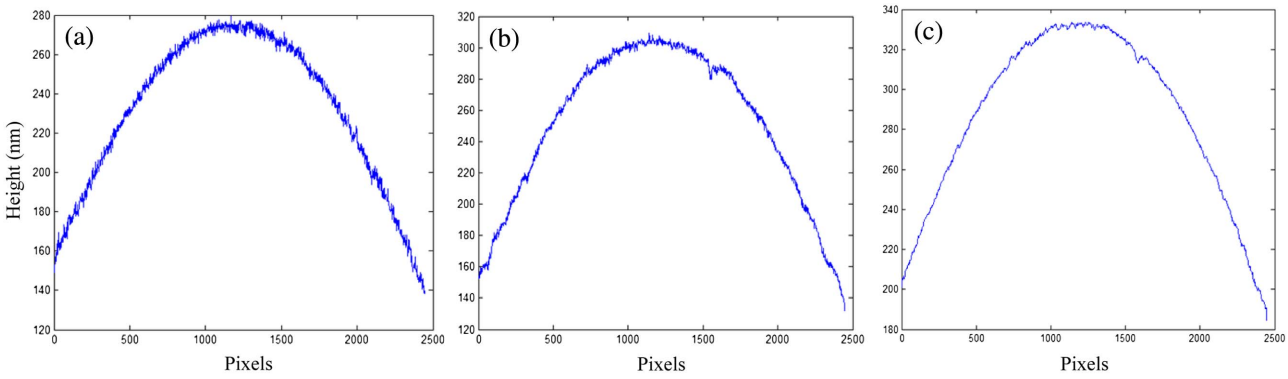

Fig. 18. Surface profiles of the spherical surface simulated by three different algorithms: (a) by using traditional WLPSI algorithm, (b) by using FFT algorithm, and (c) by using the proposed algorithm.

positions; its surface was very smooth. Due to the limited field of the optical system, only the central part of the sphere was measured.

The three algorithms were applied to the obtained interferograms with vertical scanning, and the measurement results of the spherical surface are shown in Fig. 17. It can be seen that the surface in Fig. 17(c) exhibits a less accurate profile, with noisy edges. A comparison of the results of the WLPSI, FFT, and the proposed methods is shown in Fig. 18. As shown in Figs. 18(a) and 18(b), by using WLPSI and FFT, the surface exhibits a noisier profile. This is due to the phase changes of the reflected lights caused by the coating of the spherical surface; therefore, the WLPSI method failed to detect the coherence peak and the recovered surfaces appeared uneven, while FFT could not remove the noise with frequencies close to the signal frequency. Figure 18(c) shows that the error of prediction is about several nanometers, which demonstrates the effectiveness of the proposed method. However, it can be seen that the proposed algorithm gave a good result, which was smooth and in agreement with the real condition of the spherical surface. In other words, the proposed algorithm had better immunity to environmental noises. These experiments conducted on a spherical surface also verified the quality of the proposed algorithm.

5. CONCLUSION

In this paper, what we believe is a novel surface recovery algorithm for WLI based on combined WLPSI and FFT algorithms is proposed. Based on points of discontinuity of the 3D surface identified by combining the advantages of the faster WLPSI method and the accurate localization of the FFT method, the simulated results show that the proposed algorithm performs better than the traditional WLPSI and FFT methods for determining the ZOPD positions, and improves the accuracy and anti-interference ability of the WLPSI and FFT methods. Furthermore, simulation results also show that the proposed method is highly resistant to noise and able to improve the precision and anti-interference ability, which can effectively reduce the batwing effects at the edges and solve the problem of positioning error in the maximum modulation. An optical WLSI measurement system has been introduced to verify the simulated results by the proposed algorithm. A 10 μm standard step height was measured by using the three methods in experiments, and the results show that the proposed algorithm can perform the measurement with nanometer resolution and has good repeatability and stability. In addition, experiments conducted on a spherical surface show that the proposed algorithm has better accuracy than WLPSI and

FFT to measure the surface profile, and thus these experiments demonstrate the feasibility of the proposed algorithm.

Funding. National Natural Science Foundation of China (NSFC) (61635008); National Key Research and Development Program of China (2016YFB1102203); The '111' Project by the State Administration of Foreign Experts Affairs (SAFEA); Ministry of Education of the People's Republic of China (MOE) (B07014).

REFERENCES

1. A. Townsend, N. Senin, L. Blunt, R. K. Leach, and J. S. Taylor, "Surface texture metrology for metal additive manufacturing: a review," Precis. Eng. **46**, 34–47 (2016).
2. M. Conroy and J. Armstrong, "A comparison of surface metrology techniques," J. Phys. Conf. Ser. **13**, 458–465 (2005).
3. I. Shavrin, L. Lipiainen, K. Kokkonen, S. Novotny, M. Kaivola, and H. Ludvigsen, "Stroboscopic white-light interferometry of vibrating microstructures," Opt. Express **21**, 16901–16907 (2013).
4. M. Conroy, "Interferometry advances the measurement of MEMS: scanning interferometry has the ability to obtain much information from a single noncontact measurement," Quality **49**, 24–30 (2010).
5. M. C. Park and W. K. Seung, "Direct quadratic polynomial fitting for fringe peak detection of white light scanning interferograms," Opt. Eng. **39**, 952–959 (2000).
6. P. Sandoz, R. Devillers, and A. Plata, "Unambiguous profilometry by fringe-order identification in white-light phase-shifting interferometry," J. Mod. Opt. **44**, 519–534 (1997).
7. J. H. Kim, S. W. Yoon, J. H. Lee, W. J. Ahn, and H. J. Park, "New algorithm of white-light phase shifting interferometry pursing higher repeatability by using numerical phase error correction schemes of pre-processor, main processor, and post-processor," Opt. Laser Eng. **46**, 140–148 (2008).
8. A. Gonzalez, M. Servin, J. C. Estrada, and H. C. Rosu, "N-step linear phase-shifting algorithms with optimum signal to noise phase demodulation," J. Mod. Opt. **58**, 1278–1284 (2011).
9. B. Bhushan, J. C. Wyant, and C. L. Koliopoulos, "Measurement of surface topography of magnetic tapes by Mirau interferometry," Appl. Opt. **24**, 1489–1497 (1985).
10. M. H. Shen, W. C. Wang, and C. H. Hwang, "White-light interferometer-micro-profile measurement based on higher steps phase-shifting algorithm," in *Fringe 2013—7th International Workshop on Advanced Optical Imaging and Metrology*, Berlin (Springer, 2014), pp. 341–344.
11. J. Schwider, R. Burow, K. E. Elssner, J. Grzanna, R. Spolaczyk, and K. Merkel, "Digital wave-front measuring interferometry: some systematic error sources," Appl. Opt. **22**, 3421–3432 (1983).
12. Y. Surrel, "Phase stepping: a new self-calibrating algorithm," Appl. Opt. **32**, 3598–3600 (1993).
13. S. C. Chim and G. S. Kino, "Three-dimensional image realization in interference microscopy," Appl. Opt. **31**, 2550–2553 (1992).
14. H. Muhamedsalih, X. Jiang, and F. Gao, "Comparison of fast Fourier transform and convolution in wavelength scanning interferometry," Proc. SPIE **8082**, 80820Q (2011).
15. S. Ma, C. Quan, R. Zhu, C. J. Tay, L. Chen, and Z. Gao, "Micro-profile measurement based on windowed Fourier transform in white-light scanning interferometry," Opt. Commun. **284**, 2488–2493 (2011).
16. S. Ma, C. Quan, R. Zhu, C. J. Tay, L. Chen, and Z. Gao, "Application of least-square estimation in white-light scanning interferometry," Opt. Laser Eng. **49**, 1012–1018 (2011).
17. Z. Wang, Y. Jiang, W. Ding, and R. Guo, "Fourier transform white-light interferometry based on nonlinear wavelength sampling," Opt. Eng. **52**, 104102 (2013).
18. K. G. Larkin, "Efficient nonlinear algorithm for envelope detection in white light interferometry," J. Opt. Soc. Am. A **13**, 832–843 (1996).
19. A. Harasaki, J. Schmit, and J. C. Wyant, "Improved vertical-scanning interferometry," Appl. Opt. **39**, 2107–2115 (2000).
20. P. J. De Groot, "Phase gap analysis for scanning interferometry," U.S. patent 6,989,905 (24 January 2006).
21. M. Li, C. Quan, and C. J. Tay, "Continuous wavelet transform for micro-component profile measurement using vertical scanning interferometry," Opt. Laser Technol. **40**, 920–929 (2008).
22. S. K. Debnath and M. P. Kothiyal, "Improved optical profiling using the spectral phase in spectrally resolved white-light interferometry," Appl. Opt. **45**, 6965–6972 (2006).
23. Z. Malacara and M. Servin, *Interferogram Analysis for Optical Testing*, Vol. **84** of Optical Engineering (CRC Press, 2013).
24. J. Novak, "Five-step phase-shifting algorithms with unknown values of phase shift," Optik **114**, 63–68 (2003).
25. M. Servin, J. C. Estrada, and J. A. Quiroga, "The general theory of phase shifting algorithms," Opt. Express **17**, 21867–21881 (2009).
26. Z. W. Dong, D. Nan, Y. J. Fu, H. R. Xiao, and Q. Du, "A fast Fourier transform algorithm for surface profiler based on scanning white-light interferometry," Proc. SPIE **6027**, 60270P (2006).
27. A. Hirabayashi, H. Ogawa, and K. Kitagawa, "Fast surface profiler by white-light interferometry by use of a new algorithm based on sampling theory," Appl. Opt. **41**, 4876–4883 (2002).
28. H. Muhamedsalih, F. Gao, and X. Jiang, "Comparison study of algorithms and accuracy in the wavelength scanning interferometry," Appl. Opt. **51**, 8854–8862 (2012).